

# Soft Matter

Accepted Manuscript



This is an *Accepted Manuscript*, which has been through the Royal Society of Chemistry peer review process and has been accepted for publication.

*Accepted Manuscripts* are published online shortly after acceptance, before technical editing, formatting and proof reading. Using this free service, authors can make their results available to the community, in citable form, before we publish the edited article. We will replace this *Accepted Manuscript* with the edited and formatted *Advance Article* as soon as it is available.

You can find more information about *Accepted Manuscripts* in the [Information for Authors](#).

Please note that technical editing may introduce minor changes to the text and/or graphics, which may alter content. The journal's standard [Terms & Conditions](#) and the [Ethical guidelines](#) still apply. In no event shall the Royal Society of Chemistry be held responsible for any errors or omissions in this *Accepted Manuscript* or any consequences arising from the use of any information it contains.

Cite this: DOI: 10.1039/xxxxxxxxxx

## Dynamics of cracking in drying colloidal sheets

Rajarshi Sengupta<sup>a</sup> and Mahesh S. Tirumkudulu<sup>\*a</sup>Received Date  
Accepted Date

DOI: 10.1039/xxxxxxxxxx

www.rsc.org/journalname

Colloidal dispersions are known to display a fascinating network of cracks on drying. We probe the fracture mechanics of free-standing films of aqueous polymer-particle dispersions. Thin films of the dispersion are cast between a pair of plain steel wires and allowed to dry under ambient conditions. The strain induced on the particle network during drying is relieved by cracking. The stress which causes the films to crack has been calculated by measuring the deflection of the wires. The critical cracking stress varied inversely to the two-thirds' power of the film thickness. We also measure the velocity of the tip of a moving crack. The motion of a crack has been modeled as a competition between the release of the elastic energy stored in the particle network, the increase in surface energy as a result of the growth of a crack, the rate of viscous dissipation of the interstitial fluid and the kinetic energy associated with a moving crack. There is fair agreement between the measured crack velocities and predictions.

### 1 Introduction

Thin films of drying colloidal dispersions undergo a number of complex changes. The fluid to solid transition concentrates the particles into a close packed array wherein the liquid menisci between particles at the top of the film exert compressive capillary forces on the particle network so as to shrink the film. The film being restrained by the substrate, resists deformation in the transverse direction leading to large transverse tensile stresses that cause cracks. Most studies have focused on understanding the physics of cracking on *substrates* including measurement of critical cracking stress<sup>1-6</sup>, crack spacing<sup>2,7-9</sup>, and the critical thickness of films below which they do not crack<sup>10-12</sup>. Xu et al.<sup>13</sup> have measured the stress near the tip of a propagating crack and show that the stress varies with the inverse square root of the distance from the crack-tip, while more recently, Goehring et al.<sup>14</sup> have shown that there are energy losses when a crack opens. The experiments have been complemented with theory<sup>2,12,15,16</sup> that assumes the films to be elastic and predicts the aforementioned quantities based on the Griffith's fracture criteria<sup>17</sup> for brittle materials. However, very few studies have investigated the dynamics of crack propagation. Dufresne et al.<sup>18</sup> were the first to investigate the intermittent crack motion in drying dispersions in a capillary and described the motion of the crack-tip by balancing the elastic power released to the changing surface power and the rate of viscous dissipation due to flow of fluid in pores. However, drying is accompanied by deformation of the capillary walls and

subsequent de-lamination of sections of the film which complicates the analysis<sup>19</sup>. Further, such a geometry does not allow an accurate measure of the stress that induces cracking. In order to understand the dynamics of crack propagation, it is important to accurately measure both the stress which cracks a film, and the velocity of the crack-tip.

In this work, we present novel experiments that allow measurements of both critical cracking stress and crack-tip velocity in thin free-standing films or *sheets* of drying colloidal dispersions. By eliminating the substrate, the measured quantities are dependent on the properties of the dispersion alone. Further, as demonstrated first by Inglis<sup>20</sup>, thin elastic sheets can be modeled using the plane stress approximation enabling exact theoretical treatment. Free-standing colloidal films of monodisperse polymer particles were cast between pairs of plain steel wires and the stress evolution was recorded by noting the deflection of the wires. Nucleation and subsequent time evolution of flaws were recorded under a microscope. The measured critical cracking stress scales inversely with sheet thickness, while the speed of the crack-tip is governed by a power balance involving the elastic energy, kinetic energy, surface energy and viscous dissipation. The measured critical stress and the crack tip motion is in line with theoretical predictions.

### 2 Materials and Methods

The experiments were performed using a styrene-butadiene dispersion (Styronal<sup>TM</sup> ND 811, BASF) diluted to 0.1 particle volume fraction using ultra-pure deionized water. The average particle diameter ( $2R$ ) is 185 nm, with a polydispersity index of 0.002. The experiments were performed at a temperature of 26°C(± 1°C),

<sup>a</sup> Department of Chemical Engineering, Indian Institute of Technology Powai, Mumbai, India. Fax: +91 22 2572 6895; Tel: +91 22 2576 7227; E-mail: mahesh@che.iitb.ac.in

and a relative humidity of 35% ( $\pm 5\%$ ). The experimental set-up (Fig. 1) consists of two parallel steel wires of diameter  $250\mu\text{m}$  (Gauge 10 guitar strings, JD'Addario and Co) placed at a distance of  $W = 2\text{ mm}$  from each other and strung in the middle of microscope's sample holder (Olympus IX71). Two plastic blades were placed gently on the opposite ends of the wires. The edges of the two blades were brought within 1mm of each other and a fixed volume of dispersion ( $4\text{-}30\mu\text{L}$ ) was placed between them. Translating the blades gently in opposite directions along the wires creates thin, free-standing films of varying lengths ( $6\text{-}10\text{mm}$ ).

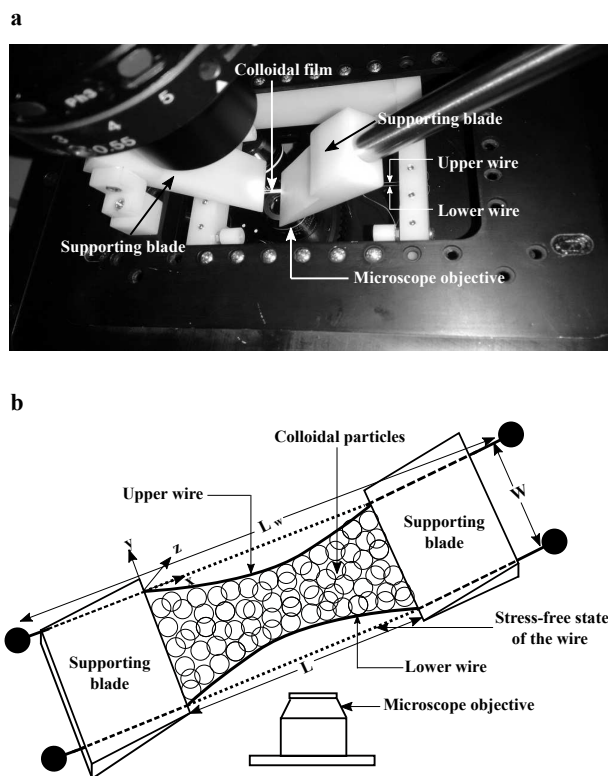


**Fig. 1** (a) The experimental set-up. (b) Schematic of the experimental set-up. Here, the length of the colloidal film is  $L$ , and the width of the film is  $W$ .

As the wet film dried, tensile stresses in the film bend the wires. The blades being thick and rigid experience negligible deflection. No deflection was observed at the two ends of the wires which were in contact with the blades. For small displacements, the deflection of a stretched wire subjected to a transverse load is given by<sup>21</sup>,

$$T \frac{d^2 Y_w}{dx^2} = -q, \quad (1)$$

where  $T$  is the tension in the wires,  $Y_w$  is the deflection of the wire along the  $y$  direction at any point  $x$  along its length, and  $q$  is the force acting per unit length on the wire. Note that  $\frac{d^2 Y_w}{dx^2}$  is the inverse radius of curvature of the wire. As will be shown later, the thickness does not vary significantly along the length of the film (i.e., along  $x$ ) so that  $q$  can be assumed to be a constant. Integrating the equation between the blade ends ( $L$ ), gives the force per unit length acting on the wire, which is equal and opposite to that acting on the film and is equal to the transverse stress in the

film multiplied by its thickness,

$$\sigma(y) = \frac{2TY_w}{L^2 h(y) \left[ \frac{x}{L} - \left( \frac{x}{L} \right)^2 \right]}, \quad (2)$$

where  $h(y)$  is the thickness of the sheet that varies along the  $y$  direction, and  $\sigma(y)h(y) = q$ . Note that  $\sigma$  refers to the normal stress in the  $y$  direction ( $\sigma_{yy}$ ). Determination of the critical cracking stress requires measurements of the tension in the wire, the maximum wire deflection ( $Y_w$  has the maximum value at  $x = L/2$ ) and the sheet thickness at the crack edge.

### 3 Experiments

#### 3.1 Measurement of wire tension

Before the start of the experiment, the blades were raised and each wire was plucked at the middle, which made it vibrate at its fundamental frequency. The vibrations of the wire were recorded using a high speed camera (Hamamatsu sCMOS C11440-22CU) at 1000 frames per second. The images were analyzed to get the frequency of vibrations. Each frame was divided into two bins, so that when the wire enters that bin, its intensity is lower than without the wire. The intensity of each bin was measured as a function of time. The vibrations in the wire cause the intensity of each frame to be different. The intensity fluctuates with the same frequency as the wire. Fast Fourier Transforms of the intensities were taken, and plotted against the frequency. The peak of the intensity corresponds to the fundamental frequency of vibration of the wire. One such result is shown in Fig. 2. The tension of a wire vibrating at its fundamental frequency is given by<sup>22</sup>

$$T = 4f^2 L_w^2 \mu, \quad (3)$$

where  $T$  is the tension in the wire,  $f$  is the frequency of vibration of the fundamental mode,  $L_w$  is the length of the vibrating wire, and  $\mu$  is the mass per unit length of the wire. The latter was determined independently by measuring the weight of different lengths of wire. For our experiments,  $L_w = 9.2\text{ cm}$ ,  $\mu = 2.9 \times 10^{-4}\text{ kg/m}$ , and  $f \sim 390\text{ Hz}$ , gave  $T \sim 1.5\text{ N}$ .

#### 3.2 Measurement of wire deflection

After the start of the experiment, the deflection of the wire due to the drying stress was measured at the center of the wire (Fig. 3). In order to achieve this, the film was cast, and then the center of one wire was focused under the microscope. To make an accurate measurement of the wire deflection, a 20X objective (0.50 NA) was used. The deflections were of the order of tens of microns. As in the case of films cast on substrates, the film begins to dry first along its boundaries. As the edges dry, the solvent flows from the center of the film towards the edges. There is very little deflection in the wires at this time. With time, sufficient solvent moves to the boundaries and evaporates, depositing the particles at the edges. This makes the central part of the film much thinner compared to the boundaries. During this time, the wires begin to show notable deflection. The deflection continues to increase till the point of fracture. Once the film cracks, the stresses in the film decrease thereby reducing the deflection in the wires.

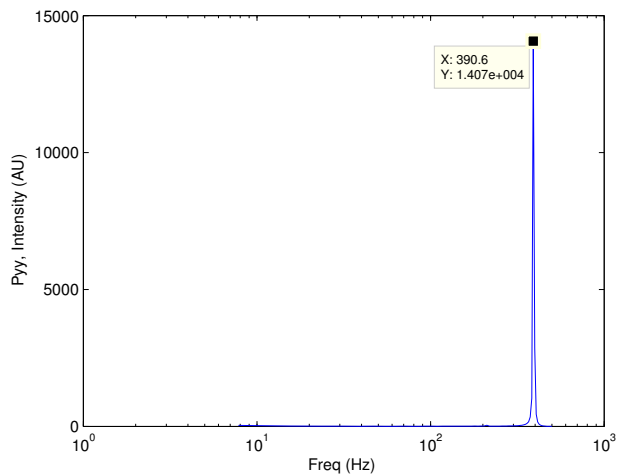


**Fig. 2** Power spectrum of intensity gives the frequency of vibration of the wire. The peak frequency value of 390.6 Hz corresponds to a tension of 1.53 N.

In many cases, the wires did not relax to their stress-free state, indicating that some residual stress remains in the film. We could not capture the deflection of the wires and the cracking of the film in the same experiment as it compromises with the accuracy of the measured deflection. However, the sudden reduction in the deflection of the wires from the point of highest deflection suggests nucleation and growth of the first crack.

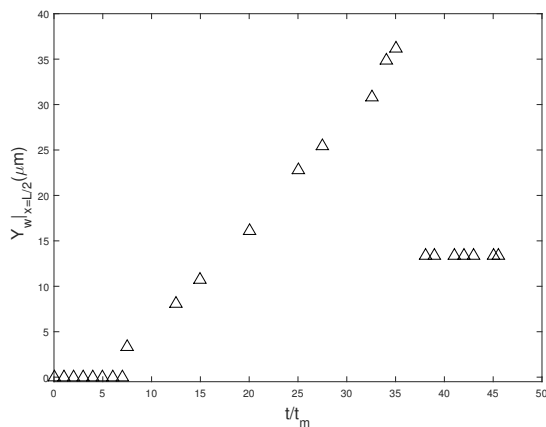


**Fig. 3** Wire deflection at  $x = L/2$  is plotted as a function of time, which is rendered dimensionless by the time at which the deflection is maximum.

### 3.3 Measurement of film thickness

After each experiment, the cracked films were collected on clean glass cover slips and their thickness measured using a profilometer (Veeco Dektak 150) both across the width starting from the crack edge and along the crack edge. Figures 4(a) and (b) show, respectively, the thickness profile of one such film along its width and its length. The thickness varies across the width of the film, being the thinnest at the crack edge, and nearly equal to the wire diameter at the edges. The film is roughly uniform along

its length ( $\pm 10\%$ ), confirming the assumption of a uniform load ( $q$ ) acting along the film.

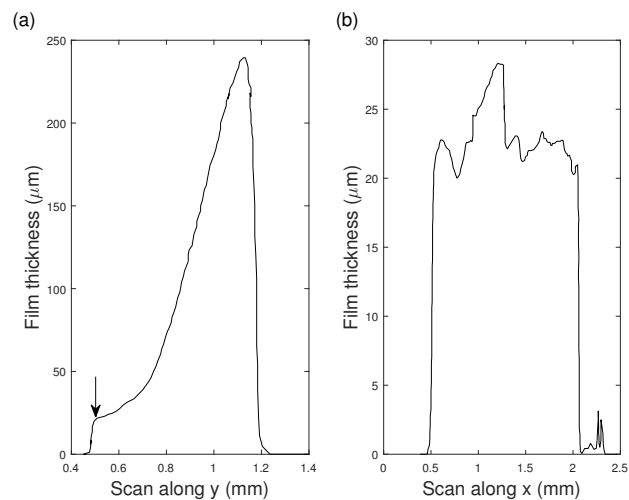


**Fig. 4** (a) Thickness profile of a part of the dried film along its width (i.e., along  $y$ ). The thickness of the film at the crack edge is approximately  $22 \mu\text{m}$  (indicated by an arrow). The film is thinnest near the center, and nearly as thick as the wire at the edge (nearly  $240 \mu\text{m}$ ). The flat region to the left of the arrow corresponds to the surface of the cover slip. (b) Thickness profile along the length (i.e., along  $x$ ) of a part of the film shows little variation, implying a constant load acts along the length of the film.

### 3.4 Cracking stress

The knowledge of wire tension, the maximum deflection and the crack edge thickness allows determination of the critical cracking stress ( $\sigma_c$ ) at the crack edge using Equation 2. Figure 5 presents the measured critical stress (filled squares), which scales approximately with the inverse two-thirds' power of the sheet thickness and is similar to those reported for cracking in films cast on substrates<sup>2,4,6</sup>. The constitutive relation for a saturated colloidal film can be approximated by the form<sup>23</sup>,  $\sigma \sim G\epsilon^2$ , where  $G$  is the shear modulus of the particles and  $\epsilon$  is the affine strain. The elastic energy recovered on the opening of a crack of length ' $c$ ' in a packing of unit thickness is,  $\sim \sigma\epsilon c^2$ . Equating this to surface energy per unit thickness of the sheet ( $\gamma c$ ) as per the Griffith's criteria<sup>17</sup> gives the critical cracking stress,  $\sigma_{c,g}c^{2/3} \sim G^{1/3}\gamma^{2/3}$ . The exact expression following detailed calculations is given by<sup>15</sup>,

$$\left(\frac{\sigma_{c,g}R}{2\gamma}\right)\left(\frac{c}{R}\right)^{2/3} = A'\left(\frac{GM\phi_{rcp}R}{2\gamma}\right)^{1/3}, \quad (4)$$

where  $\gamma$  is the surface tension of the solvent,  $M$  is the number of nearest neighbors,  $\phi_{rcp}$  is the volume fraction at random closed packing and  $A'$  is a constant equal to 0.45 for plane stress deformation. Experiments of Sarkar and Tirumkudulu<sup>24</sup> have shown that a capillary bridge of drying colloidal dispersion crack due to spherical voids/flaws trapped inside the drying bridge. The critical stress was found to follow a similar scaling with the capillary bridge diameter. Since the the flaw size was found to be a constant fraction of the bridge diameter, the theoretical scaling of  $\sigma_c \sim c^{-2/3}$  was approximately followed. If an analogous as-

sumption of the nucleating flaw size being a fraction of the film thickness ( $h$ ) is made for the present case, the experimental data can be fit by substituting  $c = 0.864h$  in equation (4) (dashed line in Fig 5). This suggests that the ideal Griffith's flaw size is of the same order as the film thickness. However, unlike the capillary bridge case, the observed flaws appear to penetrate the entire thickness and there is no constraint on the size of such a flaw in a flat film. In other words, the flaw can be many times of the film thickness. Indeed, as reported in the next section on crack dynamics, the measured sizes of the flaws which nucleate cracks were much larger, suggesting that the films crack at stresses much higher than the Griffith's stress. This is because the critical cracking stress predicted by the Griffith's criteria applies to stationary cracks under equilibrium conditions. For a flaw to increase in length, the stress must be greater than the Griffith's stress<sup>3</sup>. Figure 5 includes points that were calculated from (4) using the measured values of flaw sizes from many experiments for three thicknesses (2, 5 and 8  $\mu\text{m}$ ). Comparing them with the measurements indicates that the critical stresses can be ten times larger than the Griffith's stress.

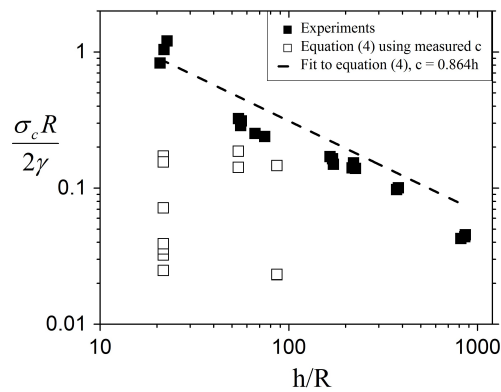


**Fig. 5** Variation of non-dimensional critical cracking stress with non-dimensional film thickness. The solid squares represent the experimentally measured critical cracking stress values, and the empty squares represent the cracking stress values as predicted by (4) using the measured values of flaw sizes just before they nucleate crack. The dashed line is a fit of the experimental data to equation 4, by assuming the flaw size,  $c$  to be a fraction of the film thickness.

### 3.5 Crack dynamics

Next, we captured the high-speed motion of the crack-tip to determine its time evolution. In these experiments, the camera was focused on the central sections of the film so as to detect the nucleation of the first crack from a flaw. A lower numerical aperture objective (4X, 0.13 NA) was used, which enabled visualization of a large area (about 3.2 mm by 0.5 mm) of the film. On casting the wet film, the intensity of the entire film is initially uniform. As drying occurs, the central part appears brighter implying that the thickness of that region reduces more than its surroundings. We attribute this to the convection of particles and fluids to the edges of the film. Eventually flaws begin to appear in the film and the crack-tip motion of the first nucleating crack was recorded. It is

important to note that in some cases, the crack nucleated outside the viewing region and such data was discarded.

Figure 6 presents images of a crack which grows very slowly between 0 and 59 ms, and then progresses rapidly in the next millisecond. Much of the growth occurs between 60-200 ms, followed by a period of slower growth and subsequent arrest. Close inspection of the crack-tip beyond 300 ms shows accumulation of water (see inset). The amount of water at the crack-tip is larger than what would be contained within a region of order  $R^2$  suggesting that water flows into the crack-tip. This observation confirms earlier predictions of a negative pressure at the crack-tip which draws the liquid from the surroundings<sup>15</sup>. Detailed recordings of the crack motion were performed with films of three different thicknesses, namely, 2, 5 and 8  $\mu\text{m}$ . At these low thicknesses, the first crack invariably occurred near the center of the film and so was easy to capture. There was significant variability in the crack evolution. For films of nearly the same thickness, the nucleating flaw size, the length to which a crack grows before stopping and the maximum value of the crack speed vary although the corresponding critical cracking stress was highly reproducible - reasons for which are not clear. The sizes of flaws that nucleate the first crack were measured from the images and the same were used to calculate the Griffith's stress (shown by empty squares in Fig. 5) using equation 4.

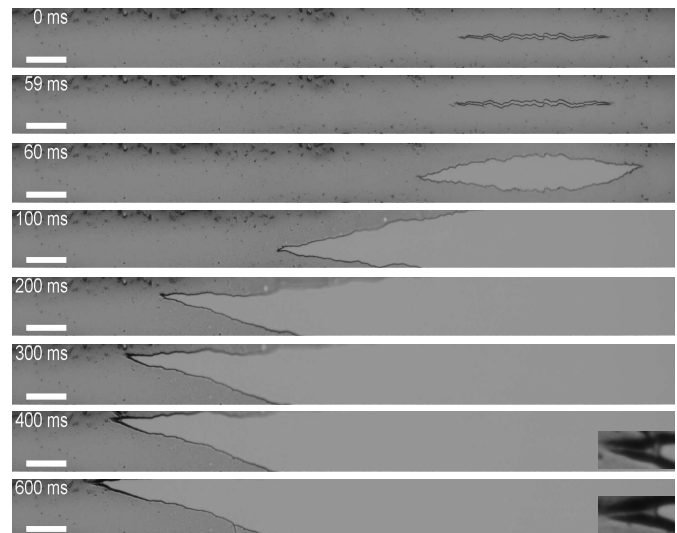


**Fig. 6** The images show the time evolution of a crack. Crack speed was determined by tracking the left side crack-tip. Emergence of a meniscus at the crack-tip at long times can be seen in the inset. The average thickness at the crack edge was 8  $\mu\text{m}$ . Scale bar: 200  $\mu\text{m}$ .

## 4 Model

The measured time evolution of crack-tip motivates a model involving an energy-rate balance, akin to the Griffith's energy balance criteria. While a detailed model for the dynamics would require accounting for the non-linear constitutive model along with detailed calculations for the various energy terms, a simpler approach of dimensional analysis applicable to a linear elastic sheet saturated with liquid is expected to provide the essence of the phenomenon. Further, the thickness varies along the  $y$ -direction,

which complicates the determination of the crack dynamics. We simplify the analysis by assuming a sheet of constant thickness, which is equal to that observed at the crack edge, and of lateral dimensions that stores the same elastic energy as in the actual film. For the actual film, the energy stored in the thicker regions will be small suggesting that most of the elastic energy is stored in the thinner regions located in the center of the film where the cracks nucleate. Recall that the thickness variations were negligible along the length of the film. The elastic energy stored in the actual film can be determined as,  $\mathcal{E}_{elas} = \int_0^W \frac{[\sigma(y)]^2}{2E} Lh(y)dy$ . On substituting the measured values of  $h(y)$  (say, from Fig. 4(a)) in the above expression for a fixed  $q$ , the effective width of a film with constant thickness (and equal to that at crack edge) containing the same elastic energy as that calculated from the above expression is about 20% of the actual width. With similar thickness variations close to both the blades, the effective area of the constant thickness film is estimated to be much less than 20% of the area of the actual film.

It should be noted that the analysis for a film with varying thickness is also possible though it is a bit involved. The thickness-averaged relation between the stress and strain for a non-uniform thickness film in the plane stress formulation is given by,<sup>25</sup>

$$\begin{aligned}\bar{\sigma}_{xx} &= \frac{E}{1-\nu^2} [\alpha_{11}\varepsilon_{xx} + \nu\alpha_{12}\varepsilon_{yy}] \\ \bar{\sigma}_{yy} &= \frac{E}{1-\nu^2} [\nu\alpha_{21}\varepsilon_{xx} + \alpha_{22}\varepsilon_{yy}] \\ \bar{\tau}_{xy} &= G\alpha_{66}\gamma_{xy}\end{aligned}$$

where the coefficients,  $\alpha_{11}$ ,  $\alpha_{12} = \alpha_{21}$ ,  $\alpha_{22}$  and  $\alpha_{66}$ , are functions of the thickness variation of the film and the over bar indicates thickness average. For a constant thickness film, these coefficients are all equal to one. For the special case of a film with constant taper, which the present case may be approximated to, Shumin et al.<sup>25</sup> show that these coefficients are constant (but different from 1). Such a case belongs to the class of anisotropic plates of constant thickness, and the expression relating the critical stress to the crack opening will have the same functional form as that for an isotropic plate of constant thickness except for a multiplying factor due to the anisotropy<sup>26</sup>. The same would be the case for the kinetic energy term to be discussed later. Since our goal is to elucidate the main aspects of the crack motion, the detailed analysis including the non-linearity of the constitutive relation along with the exact expression for the all the energy terms is postponed to future work. In what follows, we consider a constant thickness film with an area,  $A$ , equal to 15% of the area of actual film (i.e., 15% of 2mm×8mm).

The stress versus strain relation for the model linear elastic sheet containing a crack of length  $2c$  is given by<sup>27</sup>,  $\sigma = \varepsilon E_{eff}$  where  $E_{eff} = AE/(A + 2\pi c^2)$  is the effective Young's modulus of the film containing a crack, and  $E$  is the Young's modulus of the material. The strain  $\varepsilon$  applies to the deformation of the entire film as measured at the boundary. The corresponding elastic energy stored in the sheet (per unit thickness) is given by,  $\mathcal{E}_{elas} = (\varepsilon^2 E_{eff}/2)A$ . Note that with increase in  $c$ ,  $E_{eff}$  decreases leading to a decrease in  $\mathcal{E}_{elas}$  at constant strain, since the film is

held fixed at its boundaries. Combining the above relation with the Griffith's criteria for fracture<sup>17</sup>,  $\sigma_{c,g}^2 = 2E\gamma/\pi c$ , gives the locus of the Griffith's condition that relates the critical strain ( $\varepsilon_c$ ) to that corresponding to Griffith's critical stress,  $\sigma_{c,g}$ . For a fixed crack size, any stress greater than the Griffith's stress would make the system unstable, causing the crack to expand. The expression for the kinetic energy (per unit thickness of the sheet) due to the propagating crack on dimensional grounds was first proposed by Mott<sup>28</sup> and is given by,

$$\mathcal{E}_{KE} = \frac{k' \rho c^2}{2} \left( \frac{dc}{dt} \right)^2 \frac{A^2 \varepsilon^2}{(A + 2\pi c^2)^2},$$

while that for the surface energy is,  $\mathcal{E}_s = 4\gamma c$ . Here,  $k'$  is the Mott's constant,  $\rho$  is the density and  $t$  is time. Berry<sup>27</sup> equated the change in the elastic energy to the sum of the kinetic energy and surface energy to obtain an explicit expression for the crack velocity. For a fixed deformation case (constant strain case) which is applicable to the present set-up, the crack velocity increases reaching a maximum value after which it decreases to zero.

The analysis predicts crack velocities that scale with the elastic wave velocity,  $\sqrt{E/\rho}$ . The Young's modulus,  $E$ , for a colloidal packing scales as  $E \sim G\varepsilon$ , with the exact expression being<sup>15</sup>,  $E = 4GM\phi_{rcp}\varepsilon/35$ . The critical strain along with the Young's modulus can be calculated by substituting the measured values of critical stress in the constitutive relation,  $\sigma_c = E\varepsilon_c$ . Using  $G = 10^9 Pa$ ,  $M = 6$  and  $\phi_{rcp} = 0.64$ , we obtain  $\varepsilon_c \sim 10^{-2}$  and  $E \sim 10^7 Pa$ . The latter implies that the crack speeds should be  $\mathcal{O}(10^3)$  m/s, which is four orders higher than the observed value. We hypothesize the cause for the discrepancy to be the large rate of dissipation caused by flow of liquid in the pores of the colloidal sheet<sup>18</sup>. The expression for the viscous dissipation per unit thickness of the sheet is given by,  $\dot{\Phi} = \int_{\mathcal{A}} \frac{\mu}{k_p} V^2 d\mathcal{A}$ , where  $\mu$  is the viscosity of the interstitial liquid,  $k_p$  is the permeability coefficient,  $V$  is the velocity of the liquid, and  $\mathcal{A}$  is the area over which solvent flows. Since the rate of dissipation is dependent on the speed of the crack, we expect  $\dot{\Phi} \sim (\mu/k_p)(dc/dt)^2 \mathcal{A}$ .

The area  $\mathcal{A}$  is equal to the product of the crack length and a characteristic distance,  $\delta$ , from the crack face that is determined by the strength of liquid flow through the pores of the packing. Assuming that Darcy's law describes this flow<sup>29</sup>, the characteristic velocity would be,  $V = -(k_p/\mu)\nabla P \sim (k_p\gamma/\mu Rc)$ , where the pressure,  $P$ , in the pores scales with the capillary pressure,  $\gamma/R$ . However, given the relatively large crack speeds observed in our experiments (compared to the Darcy's flow velocity), the fluid flow during this time, is expected to be restricted to a small region close to the crack surface. Thus  $\delta$  should then scale with the product of the Darcy's flow velocity and the characteristic time of crack motion,  $\delta \sim (k_p\gamma/\mu Rc)/(1/c)(dc/dt)$ . The analysis assumes that the opening of the crack should significantly alter the pressure close to the crack surface resulting in dominant flow in only that region. This assumption is in line with the theoretical predictions of the pressure field for a static crack<sup>15</sup> that exhibits a singularity similar to that for the stresses close to the crack-tip. The accumulation of water close to the crack-tip at later stages of crack growth supports such an assumption. Substituting typ-

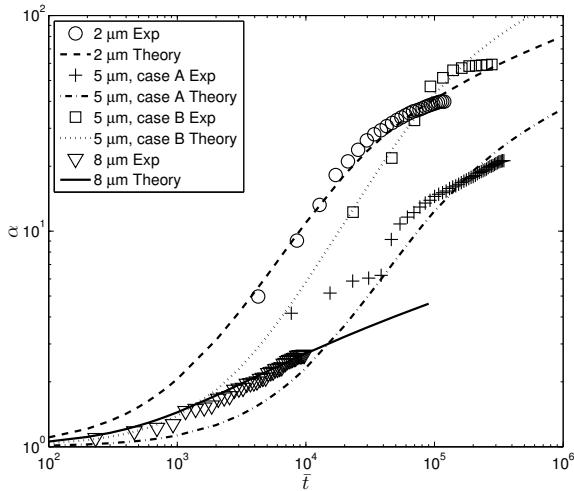


**Fig. 7** Comparison of model predictions with measurements. The parameter values, ( $c_0$ [ $\mu\text{m}$ ],  $n$ ,  $k''$ ) for the four cases in order of listing in the legend are (19, 0.07, 0.9), (26, 0.16, 2.3), (9, 0.7, 0.4), and (392, 0.026, 0.22).

ical values of parameters from our experiments, it is found that  $\delta \sim \mathcal{O}(R)$ . Thus the final expression for viscous dissipation can be written as,  $\dot{\Phi} = k'' c R (\mu/k_p) (dc/dt)^2$  where  $k''$  is a multiplicative constant.

Substituting the relevant expressions in the power balance,  $\dot{\mathcal{E}}_{elas} = \dot{\mathcal{E}}_S + \dot{\mathcal{E}}_{KE} + \dot{\Phi}$ , gives the equation of motion of the crack in its dimensionless form,

$$\ddot{\alpha} + \frac{\dot{\alpha}^2 (m - 2\alpha^2)}{\alpha (m + 2\alpha^2)} = \frac{2\pi}{k'} \frac{1}{\alpha} \left( 1 - \frac{n}{2\alpha} \frac{(m + 2\alpha^2)^2}{(m + 2)^2} \right) - \frac{2\pi k''}{k'} \frac{\dot{\alpha}}{\alpha} \left( \frac{c_0 \mu R}{\gamma k_p} \sqrt{\frac{E}{\rho}} \right) n \frac{(m + 2\alpha^2)^2}{(m + 2)^2}, \quad (5)$$

where  $\alpha(\bar{t}) = c(\bar{t})/c_0$  with  $c_0$  being the initial crack length (the flaw size that nucleates the crack),  $n = 2\sigma_{c,g}^2/\sigma_c^2 < 2$  and is calculated from Fig. 5,  $m = A/\pi c_0^2$ , and  $\bar{t} = (t/c_0)\sqrt{E/\rho}$ . In the absence of liquid flow, we recover the original equations of Berry<sup>27</sup>. The above equation is solved with the initial conditions,  $\alpha = 1$  and  $\dot{\alpha} = 0$  at  $\bar{t} = 0$ . The strength of the dissipation term depends on the dimensionless quantity,  $Q \equiv \frac{c_0 \mu R}{\gamma k_p} \sqrt{\frac{E}{\rho}}$ , which quantifies the viscous flow timescale over inertial timescale. Thus a large value of  $Q$  signifies large dissipation and therefore slower crack growth. The energy stored in the deformed wire is about three orders of magnitude lower than the elastic energy stored in the film and is thus not considered in the power balance. In our calculations,  $E = 10^7$  Pa,  $\mu = 10^{-3}$  Pa s,  $R = 92 \times 10^{-9}$  m,  $\gamma = 0.072$  N/m,  $\rho = 10^3$  kg/m<sup>3</sup> and  $k' = 1$ . The coefficient of permeability is given by,  $k_p = (1 - \phi_{rcp})^3 R^2 / (45 \phi_{rcp}^2)$ . With these values, the value of  $Q$  varied over more than an order of magnitude from  $3.6 \times 10^5$  to about  $9 \times 10^6$ . Note that the particles are hydrophilic and so the surface tension of water is taken for the calculations.

The distance of the crack tip from the center of the initial flaw was recorded as function of time and compared with the predic-

tions. Recall that in Fig 6, the flaw increased by a very small length from 0 to 59 ms followed by a rapid rise. We believe that for all times beginning from when the flaw is sighted during the drying process (which could be as far back as few minutes before 0 ms in Fig 6) to just before the rapid increase (59 ms in Fig 6), the stress remains below the critical stress value. As soon as the critical value is reached, the flaw propagates rapidly. Thus in all our calculations, the initial flaw length is taken as that just before the rapid increase in crack size. The model predictions compare well with measurements where the film thickness is taken from thickness measurements while the value of  $n$  is obtained from the critical stress measurements (Fig. 7). Further,  $k'' \sim \mathcal{O}(1)$  suggesting the correctness of the model assumptions. In all cases, the initial flaw size was obtained from experiments and corresponded to the size just before it propagated. The capillary stresses generated in the drying film drive its fracture. The physical picture is analogous to the fracture of solid sheets at constant strain<sup>27</sup>. Once the tensile stress exceeds the Griffith's stress for a static crack and reaches a critical value, a flaw nucleates a crack and starts expanding. The effective elastic modulus and hence the tensile stress and the corresponding elastic energy reduce. As the crack propagates, the kinetic energy associated with the propagating crack and the surface energy increase at the expense of the elastic energy. The predicted crack-tip increases rapidly suggesting the dominance of inertia during this early phase (Fig. 7). Subsequently, the length increases steadily. The crack-tip decelerates eventually due to increasing dissipation and surface energy, and stops moving.

At large times, there are differences in some cases since the measured crack-tips decelerate faster than predicted. We attribute the difference to the increasing accumulation of water at the moving crack-tip that further retards the motion via viscous dissipation. Experiments performed by inserting a wetting liquid between two glass strips and rupturing the film by driving in a wedge, showed significant decrease in wedge-tip speeds with viscosity<sup>30</sup>. The proposed model is only an approximate analysis and a more comprehensive model that also accounts for the non-linearity in the constitutive relation and thickness variation is expected to capture such effects.

## 5 Conclusions

The dynamics of cracking of free-standing colloidal sheets has been investigated. The critical stress which cracks such sheets has been measured experimentally, and compared with an existing theory. The motion of a crack has also been studied. There is a complex interplay of the elastic energy, surface energy, kinetic energy and viscous dissipation in crack propagation. An approximate model, including inertial effects has been developed to explain the nature of crack evolution. A more rigorous theory is required to understand the variability in crack dynamics.

## 6 Acknowledgement

RS acknowledges financial support from IIT Bombay. MST acknowledges support from the Swaranajayanti Fellowship (DST/SJF/ETA-01/2010-11).

## References

- 1 C. Petersen, C. Heldmann and D. Johannsmann, *Langmuir*, 1999, **15**, 7745–7751.
- 2 M. S. Tirumkudulu and W. B. Russel, *Langmuir*, 2005, **21**, 4938–4948.
- 3 W. Man and W. B. Russel, *Phys Rev Lett*, 2008, **100**, 198302.
- 4 K. B. Singh, G. Deoghare and M. S. Tirumkudulu, *Langmuir*, 2008, **25**, 751–760.
- 5 A. M. König, T. G. Weerakkody, J. L. Keddie and D. Johannsmann, *Langmuir*, 2008, **24**, 7580–7589.
- 6 M. Smith and J. Sharp, *Langmuir*, 2011, **27**, 8009–8017.
- 7 S. Bohn, L. Pauchard and Y. Couder, *Phys Rev E*, 2005, **71**, 046214.
- 8 C. Allain and L. Limat, *Phys Rev Lett*, 1995, **74**, 2981.
- 9 K. A. Shorlin, J. R. de Bruyn, M. Graham and S. W. Morris, *Phys Rev E*, 2000, **61**, 6950.
- 10 R. C. Chiu, T. Garino and M. Cima, *J. Am. Ceram. Soc.*, 1993, **76**, 2257–2264.
- 11 F. Doreau, G. Tari, C. Pagnoux, T. Chartier and J. Ferreira, *J. Eur. Ceram. Soc.*, 1998, **18**, 311–321.
- 12 K. B. Singh and M. S. Tirumkudulu, *Phys Rev Lett*, 2007, **98**, 218302.
- 13 Y. Xu, W. C. Engl, E. R. Jerison, K. J. Wallenstein, C. Hyland, L. A. Wilen and E. R. Dufresne, *Proc. Natl. Acad. Sci. U.S.A.*, 2010, **107**, 14964–14967.
- 14 L. Goehring, W. J. Clegg and A. F. Routh, *Phys Rev Lett*, 2013, **110**, 024301.
- 15 A. Sarkar and M. S. Tirumkudulu, *Phys Rev E*, 2011, **83**, 051401.
- 16 L. Goehring, L. Mahadevan and S. W. Morris, *Proc. Natl. Acad. Sci. U.S.A.*, 2009, **106**, 387–392.
- 17 A. A. Griffith, *Phil. Trans. R. Soc. A*, 1921, 163–198.
- 18 E. Dufresne, D. Stark, N. Greenblatt, J. Cheng, J. Hutchinson, L. Mahadevan and D. Weitz, *Langmuir*, 2006, **22**, 7144–7147.
- 19 A. Sarkar and M. S. Tirumkudulu, *Soft Matter*, 2011, **7**, 8816–8822.
- 20 C. E. Inglis, *Trans. Inst. Naval Archit.*, 1913, **55**, 219.
- 21 L. D. Landau and E. Lifshitz, *Course of Theoretical Physics*, 1986, **3**, 109.
- 22 P. M. Morse, *Vibration and Sound*, McGraw-Hill New York, 1948, vol. 2.
- 23 A. F. Routh and W. B. Russel, *Langmuir*, 1999, **15**, 7762–7773.
- 24 A. Sarkar and M. S. Tirumkudulu, *Soft Matter*, 2012, **8**, 303–306.
- 25 C. Shumin, W. Shaofu and Z. Xing., *Eng. Frac. Mech.*, 1990, **37**, 539–549.
- 26 A. Hoenig, *Eng. Frac. Mech.*, 1982, **16**, 393 – 403.
- 27 J. Berry, *J. Mech. Phys. Solids*, 1960, **8**, 207–216.
- 28 B. R. Lawn, *Fracture of brittle solids*, Cambridge university press, 1993.
- 29 W. P. Lee and A. F. Routh, *Langmuir*, 2004, **20**, 9885D9888.
- 30 S. Burns and B. Lawn, *Int J Frac Mech*, 1968, **4**, 339–345.

# GRAPHICAL ABSTRACT

## Dynamics of cracking in drying colloidal sheets

Rajarshi Sengupta & Mahesh S. Tirumkudulu

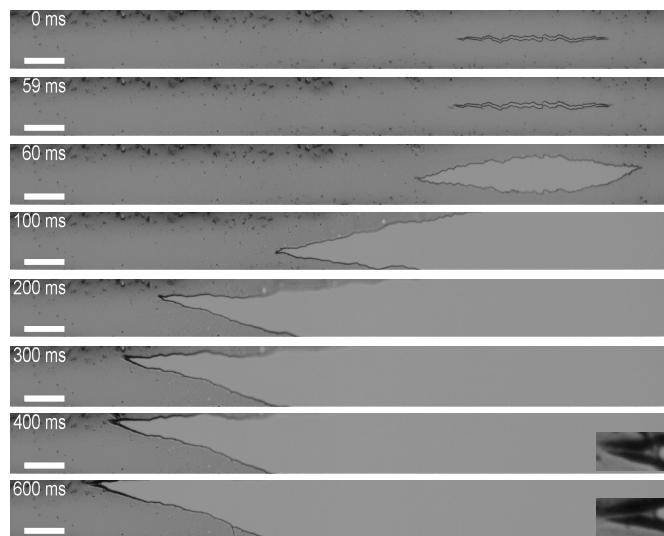


Figure 1: The images show the time evolution of a crack in a thin sheet of colloidal particles. The motion of the crack has been modeled as a competition between the release of the elastic energy stored in the particle network, the increase in surface energy as a result of the growth of a crack, the rate of viscous dissipation of the interstitial fluid and the kinetic energy associated with a moving crack. There is fair agreement between the measured crack velocities and predictions. Scale bar:  $200 \mu\text{m}$ .